JOURNAL OF SOLID STATE CHEMISTRY 21, 253–275 (1977)

Profile Analysis of Powder Neutron Diffraction Data: Its Scope, Limitations, and Applications in Solid State Chemistry

A. K. CHEETHAM

Chemical Crystallography Laboratory, 9, Parks Road, Oxford, England

AND

J. C. TAYLOR

Chemical Technology Division, Australian Atomic Energy Commission, Research Establishment, Private Mail Bag, Sutherland, N.S.W. 2232, Australia

Received November 9, 1976; in revised form January 22, 1977

Profile analysis of powder neutron diffraction data is reviewed. Applications of the technique are comprehensively tabulated and some recent examples are described in detail. Future developments and limitations of the method are also discussed, including Fourier analysis, profile refinement of X-ray data, and pulsed neutron sources.

1. Introduction

The profile method for refining powder neutron diffraction data, originally devised by Rietveld (*1*, *2*), has now become an important additional tool for the determination of crystal structure. A considerable body of experience has been gathered and it is a suitable time at which to review the achievements to date and to assess the future scope of the technique. Most of the applications have been in the field of solid state inorganic chemistry and it is with this particular area that the review is primarily concerned. Nevertheless, the literature on organic and molecular crystals has also been surveyed. The case for using powders is discussed in Section 2, and Section 3 deals with the methods of refinement. In Section 4, some recent applications of the method are described. Finally, Section 5 deals with the range and limitations of the technique and considers the directions in which it is most likely to develop.

2. The Case for Powders

2.1. X-Ray and Neutron Diffraction Analysis

Single-crystal X-ray methods have been, and will probably remain, the most important techniques for the determination of crystal structures. The phase problem can often be solved by locating a predominant scatterer in the unit cell with Patterson techniques, while direct statistical methods are now routinely used for determining structures containing only light atoms. Neutron diffraction, on the other hand, is normally used to answer specific questions about known structures, and it therefore primarily involves structure refinement rather than *ab initio* structure solution.

The weak but fluctuating dependence of neutron scattering power upon atomic number contrasts markedly with the smooth dependence shown by X rays (Fig. 1). Neutrons can therefore be used to locate very light atoms in the presence of very heavy atoms, and it is often practicable to distinguish elements which

ISSN 0022-4596

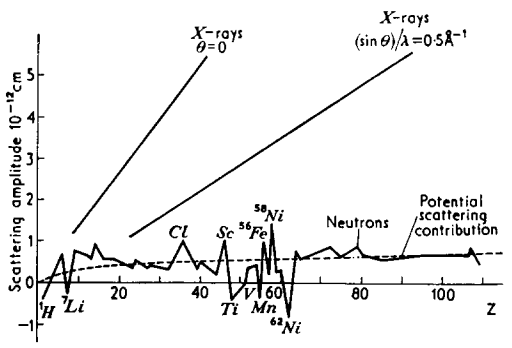

FIG. 1. The variation of neutron scattering amplitude with atomic number Z [reprinted, with permission from Ref. (*3*)].

are adjacent in the periodic table. Thus, a large proportion of the neutron diffraction literature concerns the location of hydrogen in metal hydrides and hydrogen-bonded materials, and the determination of atomic distributions in alloys or minerals. A further valuable property of the neutron is its magnetic moment. This leads to additional scattering from materials containing paramagnetic ions, and in the case of magnetically ordered compounds, additional peaks may appear in the diffraction pattern.

Neutron beams are many times weaker than X-ray beams so that neutron diffraction samples are generally larger than those required for X-ray studies; a single crystal is usually 20–100 mm^3 in volume for neutron diffraction compared with 0.1 mm^3 or smaller for X rays. We should note, however, that with a high-flux beam reactor (HFBR), neutron measurements are possible with crystals as small as 1 mm^3. It is nevertheless true that the main limitation in neutron diffraction studies until the present time has been the need for large crystals.

2.2. *Single Crystals or Powders?*

Single-crystal data collection using either X rays or neutrons is now relatively routine in nature. A computer controls the movement of the crystal from one reflecting position to another and can also be used to determine the orientation matrix and lattice parameters. In principle, no preliminary photographic examination of the crystal is necessary, although its omission can clearly lead to problems. Given the intrinsically greater information content of single-crystal data, structural studies by powder techniques would be almost unnecessary were it not for the difficulties encountered in the preparation of single crystals. This restriction is particularly evident in neutron studies where we have seen that larger crystals are required. Consequently, powder measurements often afford the only means of solving a structural problem for which neutrons are required.

Data collection for powder neutron diffraction is essentially very simple and computer control of the instrument is unnecessary. A typical experimental arrangement is shown in Fig. 2. The time for data collection may vary between several hours and several days depending primarily on the incident flux, the sample size, and the instrumental resolution. A monochromatic neutron beam is normally used with a mean wavelength of 1.0–2.5 Å. The sample (1–10 g) is contained in a cylindrical can, usually made of vanadium (the

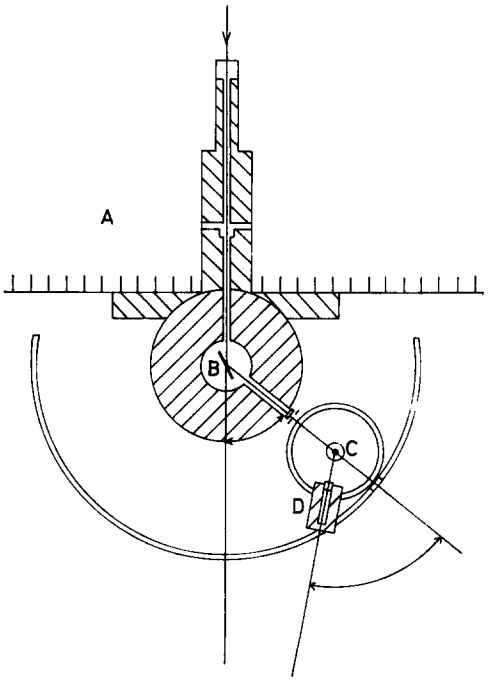

FIG. 2. Schematic layout of a neutron powder diffractomer; A, reactor; B, monochromator; C, sample; D, counter.

coherent scattering length of vanadium is almost zero) or a null matrix alloy of Ti and Zr. For corrosive samples, thin-walled Kel-F tubes of 15-mm diameter are suitable; Kel-F gives one broad diffraction peak at $\sin\theta/\lambda = 0.09$ and this can be excluded from the analysis. For air-sensitive materials, sealed quartz tubes are often convenient.

A distinct advantage of powders is that twinning and secondary extinction effects, which may hamper single-crystal studies, are essentially absent. Preferred orientation, which can be a serious source of error in X-ray powder work where the sample volume is small, is much less severe with neutrons. If preferred orientation effects are detected, then a correction may be applied or the orientation of the crystallites may be further randomized by mixing with an excess of, say, MgO.

The most striking advantage of powder neutron diffraction is the ease with which data can be collected over a wide range of temperatures. Experiments are carried out routinely at temperatures down to 4.2°K and intensity measurements have been carried out without difficulty up to 1450°K (*4*). This advantage arises for two reasons. First, variable temperature measurements are more readily performed with powders than single crystals because it is not necessary to move the sample during data collection. Second, neutrons have an advantage over X rays because the neutron absorption cross sections of most elements are typically 10^4 times smaller than the X-ray cross sections (*3*). Consequently, the structure of the cryostat or furnace has a minimal effect upon the diffraction experiment. For the same reasons powder neutron diffraction is very suitable for examining samples held in high-pressure cells (*5*).

Clearly, powders have much to offer the crystallographer but we should not disguise the fact that powder measurements do not provide as much information as single-crystal studies. Except for the case of simple materials of high symmetry, we are mainly restricted to the *refinement* of structures; a starting model must be obtained by other means. This limitation is not discouraging, however, because even single-crystal neutron measurements are rarely used for the solution of structures. More serious is the loss of information due to the overlap of adjacent reflections in the pattern The question then arises, How do we obtain the maximum amount of information from a powder diffraction profile?

3. Refinement Methods in Powder Neutron Diffraction

3.1. Traditional Powder Refinement—the Integrated Intensity Method

The traditional approach to the refinement of powder data has been to reduce the pattern to a set of integrated intensities, i.e., line data, and then to $\sum F_k^2$ values, F_k being the customary structure factor and the $\sum$ denoting a summation for overlapping reflections. Some workers have included in least-squares refinements only those Bragg reflections which are not superposed, and they have utilized programs such as ORFLS (*6*). Others have used programs which do include the effect of overlapping (*7–9*). In either case, information is lost in terms of the shape of the envelope corresponding to each $\sum F_{hkl}^2$ value. For structures of low symmetry, the overlapping soon becomes severe and refinement by this method becomes impracticable.

3.2. The Rietveld Profile Refinement Program

In 1967 Rietveld (*1*) introduced the "Profile Refinement" technique, following his short note with a detailed description of a computer program in 1969 (*2*). Instead of using line data, Rietveld fitted the structural parameters to the overall profile of the powder pattern, assuming the pattern to be the sum of a number of Gaussian-shaped Bragg reflections centered at their respective Bragg angle positions. The data are not artificially compressed as in the conventional method, but the actual point intensity counts are used as the least-squares data input. This is a more natural representation of the available intensity data, and leads to a greater efficiency of information retrieval from the superposed reflections in the pattern.

The Rietveld program minimizes the quantity:

$$M = \sum_i w_i \{ Y_i(\text{obs}) - (1/c)\, Y_i(\text{calc}) \}^2$$

where Y_i is the background-corrected intensity at a 2θ point i, c is a scale factor, and w_i is a least-squares weight, equal to $(\sigma_i^2)^{-1}$. Y_i (calc) is formed by summing the contributions from all Bragg reflections which overlap at point i, the contribution dropping to zero when $|2\theta_i - 2\theta$ (Bragg)| is greater than 1.5 H_k. H_k is the full-width at half-height of the Bragg reflection k being considered. Rietveld assumes that the variation of H_k^2 with angle can be represented by a three-term power series in $\tan\theta$:

$$H^2 = U\tan^2\theta_k + V\tan\theta_k + W,$$

where U, V, and W are half-width parameters. The contribution Y_i of a Bragg peak to the measured intensity at position $2\theta_i$ is

$$Y_i = t\cdot F_k^2\cdot j_k\cdot L_k\cdot 2(\ln 2)^{1/2}/H_k\pi^{1/2} \times \exp[(-4\ln 2/H_k^2)(2\theta_i - 2\theta_k)^2],$$

where

t = the step-width of the counter,
j_k = the multiplicity of the reflection,
L_k = the Lorentz factor,
$2\theta_k$ = calculated position of the Bragg peak, corrected for the zero point shift of the counter.

This can be rewritten simply as

$$Y_i = W_{i,k}F_k^2,$$

where $W_{i,k}$ is a measure of the contribution of a Bragg reflection at position $2\theta_k$ to the profile at position $2\theta_i$. Where more than one reflection contributes to the profile intensity at point i, we have

$$Y_i(\text{calc}) = \sum_k W_{i,k}F_k^2.$$

It is fortunate that, because of their simple geometry, neutron powder diffractometers give peaks whose shapes are accurately described by a Gaussian function. The structural and half-width parameters, the zero point error in the counter setting, and the unit cell dimensions are all included as variables in the least-squares refinements. There is also provision for correcting preferred orientation effects in the case of plate-like crystals which tend to align their normals along the axis of the sample can. In addition, the standard Rietveld program refines magnetic structures.

The R-factors quoted in profile analysis are defined as follows:

$$R_p = \sum|Y_i(\text{obs}) - (1/c)\,Y_i(\text{calc})|/\sum|Y_i(\text{obs})|,$$

and

$$R_{pw} = [\sum w_i(Y_i(\text{obs}) - (1/c)\,Y_i(\text{calc}))^2/\sum w_i\,Y_i(\text{obs})^2]^{1/2}.$$

It should be noted that these R-factors are typically around 0.10 (10%) since they are based upon the statistics of *point* intensities rather than integrated intensities or structure factors.

Rietveld (*1*) carried out integrated intensity and profile refinements on the same set of neutron powder data for WO_3, and found that the profile method reduced the standard deviations by an average factor of 2.3. With an improved set of data using a longer wavelength, Loopstra and Rietveld (*10*) reduced the original standard deviations by a factor of 4.8.

Several modifications of the original Rietveld program are now available, including one for the refinement of anisotropic temperature factors (Sect. 4.5) and a version in which flexible molecular constraints have been introduced (Sect. 5.2). The modification of the program to handle X-ray powder data is also described (Sect. 5.5).

4. Some Applications of Neutron Powder Profile Analysis

The most important consequence of profile analysis is that it has extended the scope of powder studies to include systems of low crystallographic symmetry. Indeed, unit cells of low symmetry are preferred since the incidence of completely juxtaposed reflections is reduced. Most of the compounds studied to date by profile analysis of powder neutron diffraction data are listed in Table I.

It is evident that profile analysis has already made a significant contribution to our understanding of crystalline materials, particularly in the field of solid state inorganic chemistry. In this section of the review we have selected a small number of examples to illustrate the range and limitations of the method in a variety of solid state problems. In Section 4.2 we describe some applications to the structural

TABLE I

COMPOUNDS STUDIED BY PROFILE ANALYSIS OF POWDER NEUTRON DIFFRACTION DATA

Class	Compound	Number of positional parameters	Space group	Unit cell volume (Å^3)	R_p-factor (Sect. 3.2)	Reference
Binary halides	CuF_2[a]	3	$P2_1/c$	68.7	0.06	*11, 12*
	FeF_3[a]	1	$R\bar{3}c$	103.8	0.05	*13*
	YF_3	7	*Pnma*	191.4	0.08	*14*
	BiF_3	7	*Pnma*	222.9	0.09	*14*
	LaF_3	5	$P\bar{3}c1$	328.6	0.06	*15*
	CeF_3	5	$P\bar{3}c1$	320.9	0.13	*15*
	TlF	7	*Pm2a*	173.6	—	*16*
	UCl_3	2	$P6_3/m$	207.3	0.08	*17*
	UBr_3	2	$P6_3/m$	242.6	0.10	*18*
	UI_3	4	*Ccmm*	605.8	0.15	*19*
	UCl_4	2	$I4_1/amd$	508.5	0.12	*20*
	UBr_4	9	$C2/m$	667.0	0.15	*21, 22*
	MoF_6 (193°K)	12	*Pnma*	415.5	0.11	*23*
	WF_6 (193°K)	12	*Pnma*	422.0	0.08	*24*
	UF_6 (193°K)	12	*Pnma*	454.2	0.08	*25*
	MoF_6 (290°K)	1	*Im3m*	240.8	0.10	*26*
	WF_6 (290°K)	1	*Im3m*	250.0	0.13	*27*
	UF_6 (290°K)	12	*Pnma*	461.9	0.13	*28, 25*
	β-WCl_6	7	$P\bar{3}m1$	546.3	0.12	*29*
	UCl_6	7	$P\bar{3}m1$	625.0	0.16	*30*
Mixed halides	Cs_2CrCl_4[a]	2	$I4/mmm$	447.5	0.11	*31*
	K_2MnF_4[a]	2	$I4/mmm$	230.4	—	*32*
	Li_2MnCl_4	3	$Fd3m$	1159	0.06	*33*
	$Na_2Mn_3Cl_8$	4	$R\bar{3}m$	943.2	0.12	*34*
	Na_6MnCl_8	1	$Fm3m$	1415	0.08	*34*
	$CsCoCl_3 \cdot 2H_2O$[a]	15	*Pcca*	715.6	—	*35*
	K_2NiF_6	1	$Fm3m$	533.2	0.16	*36*
	Rb_2CuCl_4	4	*Cmca*	803.5	—	*37*
	Rb_2CuCl_3Br	4	*Cmca*	828.7	—	*37*
	$Rb_2CuCl_2Br_2$	4	*Cmca*	854.5	—	*37*
Oxyhalides	CrOCl[a]	3	*Pmmn*	94.6	—	*38*
	$UOCl_2$	24	*Pbam*	1086	0.14	*39*
	UO_2Cl_2	9	*Pnma*	419.8	—	*40*
	$UO_2Cl_2 \cdot H_2O$	18	$P2_1/m$	275.6	0.12	*41*
	$UO_2Cl_2 \cdot D_2O$	18	$P2_1/m$	276.2	0.12	*41*
Binary oxides and hydroxides	$D_2O \cdot 11Al_2O_3$ (4.5 and 823°K)	13	$P6_3/mmc$	614.3	0.15	*42*
	FeOOH[a]	7	$P2_1nm$	65.5	—	*43*
	Y_2O_3	4	*Ia3*	1192	0.06	*44*
	NbO_2	18	$I4_1/a$	1122	0.11	*45*

[a] Nuclear and magnetic structure refinement.
[b] Data collection under high pressure.
[c] Neutron polarization analysis.

TABLE I—*Continued*

Class	Compound	Number of positional parameters	Space group	Unit cell volume (Å^3)	R_p-factor (Sect. 3.2)	Reference
	TeO_2 (1 bar)	4	$P4_12_12_1$	175.5	—	*46*
	TeO_2[b] (19.8 kbar)	9	$P2_12_12_1$	168.4	—	*46*
	Pr_7O_{12}	9	$R\bar{3}$	293.0	0.13	*47*
	Nd_2O_3	2	$P\bar{3}m1$	—	0.07	*48*
	TbO_2	0	$Fm3m$	142.6	0.10	*49*
	WO_3	24	$P2_1/n$	422.9	—	*10*
	Bi_2O_3	15	$P2_1/c$	330.2	—	*50*
	α-U_3O_8	3	$P\bar{6}2m$	166.5	—	*51*
	β-U_3O_8	10	$Cmcm$	671.8	—	*52*
	$D_2U_3O_{10}$	21	$P\bar{1}$	212.3	0.16	*53*
Mixed oxides	$TiNb_2O_7$	28	$A2/m$	796.4	0.09	*54*
	ortho-$Ti_2Nb_{10}O_{29}$	41	$Amma$	2178	0.11	*54*
	$BaTiO_3$	3	$R3m$	64.0	—	*55*
	$DyCrO_3$[a]	7	$Pbnm$	220.2	—	*56*
	$Ba_{0.5}Sr_{0.5}MnO_{2.84}$	2	$P6_3/mmc$	246.9	0.11	*57*
	$Ba_{0.1}Sr_{0.9}MnO_{2.96}$[a]	2	$P6_3/mmc$	235.3	0.11	*57*
	$La_{1-x}Ba_xMn_{1-y}Ti_yO_3$	7	$Pnma$	244.7	—	*58*
	α-$NaFeO_2$[a]	1	$R\bar{3}m$	127.5	—	*59*
	$BaFeO_{2.79}$	5	$P6_3/mmc$	390.0	0.13	*60*
	$BiFeO_3$[ac]	6	$R3c$	123.4	0.08	*61*
	$Sr_2Fe_2O_5$[a]	9	$Icmm$	488.8	0.09	*62*
	$BaCoO_{2.6}$	—	$P6_3/mmc$	—	—	*63*
	$GeO_2 \cdot 9Nb_2O_5$	18	$I4/m$	947.6	0.10	*64*
	$NaNbO_3$	15	$Pbma$	475.6	—	*65*
	$KNbO_3$ (tet.)	3	$P4mm$	64.9	—	*66*
	$KNbO_3$ (ortho.)	5	$Amm2$	129.3	—	*66*
	$KNbO_3$ (rhombo.)	4	$R3m$	64.8	—	*66*
	$Na_{1-x}K_xNbO_3$	9	Pm	239.4	—	*67*
	$NiNb_2O_6$[a]	—	$Pbcn$	—	—	*68*
	$Ba_4Sb_3LiO_{12}$	1	$Im3m$	554.8	0.06	*69*
	$Ba_3Ta_2ZnO_9$	4	$P\bar{3}m1$	205.5	0.08	*70*
	$Ba_4Ta_3LiO_{12}$	6	$P6_3/mmc$	554.7	0.11	*71*
	$Ba_5W_3Li_2O_{15}$	9	$P6_3/mmc$	680.6	0.09	*72*
	Fe_2WO_6[a]	—	$Pbcn$	—	—	*68*
	$BaPbO_3$	3	$Imma$	308.4	0.11	*73*
	$BaBiO_3$	7	$I2/m$	328.8	0.06	*74*
	$CaUO_3$	2	$R\bar{3}m$	228.7	0.05	*75*
	$SrUO_4$	8	$Pbcm$	356.0	0.11	*75*
	$BaUO_4$	8	$Pbcm$	385.8	0.13	*75*
	Ca_2UO_5	21	$P2_1/c$	466.6	0.13	*75*
	Sr_2UO_5	21	$P2_1/c$	517.1	0.10	*75*
	Ca_3UO_6	29	$P2_1$	283.1	0.11	*75*
	Sr_3UO_6	29	$P2_1$	315.0	0.12	*75*
	$Ca_3Cr_2(GeO_4)_3$[a]	3	$Ia3d$	1842	—	*76*
	$Al_2Mn_3(SiO_4)_3$[a]	3	$Ia3d$	1569	—	*77*
	$Al_2Mn_3(GeO_4)_3$[a]	3	$Ia3d$	1683	—	*77*
	$Ca_3Fe_2(GeO_4)_3$[a]	3	$Ia3d$	1872	—	*78*
	$Tb_3Fe_5O_{12}$[a]	3	$Ia3d$	1923	0.08	*49*

TABLE I—*Continued*

Class	Compound	Number of positional parameters	Space group	Unit cell volume (Å^3)	R_p-factor (Sect. 3.2)	Reference
Chalcogenides and pnictides	VAs^a	2	*Pnam*	123.8	—	*79*
	$Cr_2S_3{}^a$	2	$R\bar{3}$	509.0	—	*80*
	$CrAs^a$	4	*Pnma*	121.5	—	*81*
	$CrSb_2{}^a$	2	*Pnnm*	135.5	—	*82*
	$MnBi^a$	3	$P222_1$	193.8	—	*83*
	$MnBi_{0.9}Sb_{0.1}{}^a$	3	$P222_1$	184.1	—	*83*
	$Mn_{0.9}Fe_{0.1}As$	4	*Pnma*	—	—	*84*
	$Fe_3Se_4{}^a$	6	$I2/m$	246.1	—	*85*
	$FeAs^a$	4	*Pnma*	110.4	—	*86*
	$FeSb_2$	2	*Pnnm*	—	—	*82*
	$CoAs^a$	4	*Pnma*	108.3	—	*87*
	$Ni_{1.67}Te_2$	1	$P\bar{6}2m$	72.3	0.06	*88*
	$NiTe_2$	1	$P\bar{6}2m$	67.7	0.06	*88*
	CeS^a	0	$Fm3m$	191.8	0.13	*89*
	NdS^a	0	$Fm3m$	184.4	0.05	*89*
	$NdSe^a$	0	$Fm3m$	204.4	0.10	*89*
	$NdTe^a$	0	$Fm3m$	224.4	0.11	*89*
	$TbSe^a$	0	$Fm3m$	187.2	0.07	*89*
	NdN^a	0	$Fm3m$	132.7	0.17	*90*
	NdP^a	0	$Fm3m$	198.7	0.10	*90*
	$NdAs^a$	0	$Fm3m$	211.9	0.05	*90*
	$NdSb^a$	0	$Fm3m$	252.0	0.08	*90*
	$LiVS_2$	1	$P\bar{3}m1$	58.2	—	*91*
	$LiCrS_2{}^a$	1	$P\bar{3}m1$	62.7	—	*91*
	$NaCrS_2{}^a$	1	$R\bar{3}m$	213.3	—	*92*
	$KCrS_2{}^a$	1	$R\bar{3}m$	235.9	—	*93*
	$CuCrS_2$	3	$R3m$	196.3	—	*92*
	$AgCrS_2$	3	$R3m$	217.0	—	*92*
	$NaCrSe_2{}^a$	1	$R\bar{3}m$	246.1	—	*92*
	$AgCrSe_2{}^a$	3	$R3m$	248.9	—	*92*
	$M_{0.25}NbS_2{}^a$ (M = Cr, Mn)	4	$P6_3/mmc$	472.2 (Mn)	—	*94*
	$M_{0.33}NbS_2{}^a$ (M = V, Mn, Fe, Co, Ni)	5	$P6_3/mmc$	366.3 (Mn)	—	*94*
	$Mn_{0.25}TaS_2{}^a$	4	$P6_3/mmc$	480.0	—	*94*
	$M_{0.33}TaS_2{}^a$ (M = Fe, Co, Ni)	5	$P6_3/mmc$	349.0 (Fe)	—	*94*
Metals and alloys	Ni	0	$Fm3m$		—	*95*
	$PrZn^a$	0	$Pm3m$	50.1	—	*96*
	$NdZn^a$	0	$Pm3m$	49.3	—	*96, 97*
	$NdMg^a$	0	$Pm3m$	57.9	—	*96*
	$NdAg^a$	0	$Pm3m$	51.4	—	*96*
	$Tm_2Fe_{17}{}^a$	5	$P6_3/mmc$	509.1	—	*98*
	$ThNi_{5-5x}Co_{5x}{}^a$	0	$P6/mmm$	86.6	0.05	*99*
	$ThFe_{5-5x}Ni_{5x}{}^a$	1	$P\bar{3}m1$	91.3	0.08	*100*

TABLE I—*Continued*

Class	Compound	Number of positional parameters	Space group	Unit cell volume (Å^3)	R_p-factor (Sect. 3.2)	Reference
Hydrides	LaD_{2+x}	5	$I4_1md$	359.7	0.09	*101*
	CeD_{2+x}	5	$I4_1md$	338.8	0.08	*101*
	PrD_{2+x}	5	$I4_1md$	334.4	0.14	*101*
	$LaCo_5D_{3.35}$	2	*Cmmm*	198.6	0.08	*102*
	$PrCo_5D_{3.6}$	2	*Cmmm*	193.4	0.06	*102*
	$PrCo_5D_{2.9}$	5	*Im2m*	376.2	0.07	*102*
	$NdCo_5D_{2.8}$	5	*Im2m*	373.4	0.12	*102*
	$CeCo_5D_{2.55}$	3	*Ccmm*	363.0	0.09	*102*
Miscellaneous (inorganic)	$(NH_4)H_2PO_4$ (tet.)	3	$I\bar{4}2d$	423.2	—	*103*
	$(NH_4)H_2PO_4$ (ortho.)	6	$P2_12_12_1$	420.8	—	*103*
	KCN[b] (22 kbar, 347°K)	1	*Pm3m*	55.2	—	*104*
	KCN[b] (25 kbar, 296°K)	4	*Cm*	107.6	—	*104*
	$Ca(ND_3)_6$	6	*Im3m*	732.4	0.11	*105*
	$Fe_4[Fe(CN)_6]_3 \cdot 14D_2O$ (Prussian Blue)	7	*Fm3m*	1046	0.07	*106*
	$D_3Co(CN)_6$	4	$P\bar{3}m1$	204.5	0.10	*107*
	$KIO_3 \cdot HIO_3$	6	$P2_1/c$	1247	0.07	*108*
	$Ni(IO_3)_2 \cdot 2D_2O$[a]	21	*Pbca*	736.0	0.07	*109*
	TaON	9	$P2_1/c$	127.2	0.13	*110*
Miscellaneous (organic)	C_2D_2	4	*Acam*	206.0	0.08	*111*
	$(C_2H_4)_n$ Polyethylene	6	*Pnma*	88.0	—	*112*
Appendix	NaO_2 (293°K)	1	*Fm3m*	167.5	0.10	*141*
	NaO_2 (4.2°K)	2	*Pnnm*	80.5	0.14	*141*
	Mg	0	$P6_3/mmm$	—	—	*142*
	$MgAl_2O_4$	1	*Fd3m*	—	—	*143*
	SF_6	1	*Im3m*	206.9	0.08	*144*
	CaF_2 (high temperature)	0	*Fm3m*	—	—	*145*
	CrOOH	7	*Pnnm*	62.6	0.05	*146*
	CrOOD	7	*Pnnm*	62.5	0.06	*146*
	$MnNb_2O_6$[a]	—	*Pbcn*	—	—	*147*
	$Mn(Nb_{0.85}Ta_{0.15})_2O_6$[a]	—	*Pbcn*	—	—	*147*
	$MnTa_2O_6$[a]	—	*Pbcn*	—	—	*147*
	CoMnSi[a]	6	*Pnma*	147.2	—	*148*
	SrF_2 (high temperature)	0	*Fm3m*	~205	—	*145*
	$SrZrO_3$	6	*Pbnm*	275.8	0.13	*149*
	β-Nb_2N	0	$P\bar{3}1m$	119.8	0.11	*150*
	γ-NbN	5	$P4/m$	656.6	0.09	*150*
	$Cs_2LiCr(CN)_6$	7	$P4/mnc$	622.5	—	*151*
	CsO_2	1	$I4/mmm$	147.3	0.13	*141*
	BaF_2 (high temperature)	0	*Fm3m*	~250	—	*145*
	γ-UO_3 (373°K)	7	$I4_1/amd$	951.4	0.06	*152*
	γ-UO_3 (293°K)	10	*Fddd*	1893	0.10	*152*

chemistry of uranium and in Section 4.3, other measurements involving the location of light atoms are discussed. Section 4.4 details some determinations of atomic distributions, while phase transitions are considered in Section 4.5. In Section 4.6 a structure solution by the combination of profile analysis and high-resolution electron microscopy is described.

But, how reliable is profile analysis and how do the results compare with those determined by single-crystal X-ray methods? This important question is considered in Section 4.1.

4.1. X-ray and Neutron Study of $GeO_2 \cdot 9Nb_2O_5$

Germanium–niobium oxide of approximate composition $GeO_2 \cdot 9Nb_2O_5$ has a block structure of the type common to compounds based upon Nb_2O_5. In this particular example, columns of the ReO_3 structure, 3×3 octahedra in cross section, are linked to identical columns by MO_6 octahedra sharing edges (Fig. 3). The structure is apparently the same (*113*) as that of PNb_9O_{25} ($M_{10}O_{25}$), a surprising result since the stoichiometry of the mixed oxide is $M_{10.11}O_{25}$. Nonstoichiometry is unexpected in the niobium oxides since they normally appear almost infinitely adaptable to new stoichiometries by altering the size and arrangement of the blocks. For this reason, the structure of $GeO_2 \cdot 9Nb_2O_5$ has recently been examined by single-crystal X-ray diffraction, powder neutron diffraction, and electron microscopy (*64*).

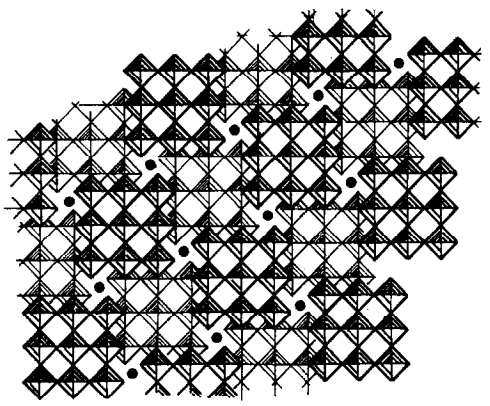

FIG. 3. The idealized structure of $GeO_2 \cdot 9Nb_2O_5$. MO_6 octahedra with thick and thin outlines have M at $z = 0$ and $z = \frac{1}{2}$, respectively. Filled circles represent tetrahedral tunnel sites (*64*).

The origin of the nonstoichiometry lies in the partial occupancy of a new type of interstitial site (Nb4) in the tunnels defined by four adjacent columns. These tunnels normally contain only tetrahedrally coordinated metal atoms. The new site was readily found by Fourier analysis of the X-ray data. The limitation of the powder method is clearly illustrated by our initial inability to locate this new site with its partial occupancy of only 0.10. However, when the site was included in the powder refinement, the R-factor fell from 10.7 to 9.8%.

The power of profile analysis for refining structures is readily appreciated when the final atomic coordinates from the single-crystal and powder studies are compared (Table II). The single-crystal data were collected on a automatic diffractometer and 1224 symmetry independent reflections were analyzed, each intensity being the mean of four measured equivalents. The final X-ray R-factor was 3.4% (based upon structure factors). The parameters from the single-crystal study have smaller standard deviations than those from the neutron work. Of the 17 positional parameters, however, only one differs by more than three standard deviations, as between the two analyses, and 10 are within one standard deviation.

4.2. Uranium Crystal Chemistry

Since neutron diffraction facilities are, of necessity, located at nuclear reactor installations, it is not surprising that profile analysis has already been extensively applied to studies on uranium compounds (see Table I). The obvious advantage of using neutrons to probe structures containing uranium lies in the greater precision with which the lighter atoms may be located. In a relatively short space of time, accurate atomic coordinates for many uranium halides and oxyhalides have been obtained in the Chemical Technology Division, Lucas Heights. Most of the structures had not previously been elucidated in detail because of the difficulty in obtaining single crystals. Thus, only the uranium positions in UCl_3, UCl_4, UCl_6, UBr_3, and UI_3 were definitely known from the early X-ray powder

TABLE II

COMPARISON OF SINGLE-CRYSTAL X-RAY AND POWDER NEUTRON STUDIES ON $GeO_2 \cdot 9Nb_2O_5$[a,b]

	x Coordinates		*y* Coordinates	
	X rays	Neutrons	X rays	Neutrons
Ge	0.0	0.0	0.5	0.5
Nb_1	0.0	0.0	0.0	0.0
Nb_2	0.21826(2)	0.2191(6)	0.10546(3)	0.1060(8)
Nb_3	0.11750(3)	0.1173(7)	0.32575(3)	0.3246(6)
Nb_4	0.44338(30)	0.4394(44)	0.03048(29)	0.0292(64)
01	0.0	0.0	0.0	0.0
02	0.2496(2)	0.2484(7)	0.3884(2)	0.3893(9)
03	0.1171(2)	0.1183(9)	0.0492(2)	0.0482(9)
04	0.1758(2)	0.1758(9)	0.2154(2)	0.2157(7)
05	0.0130(2)	0.0131(8)	0.2814(3)	0.2832(8)
06	0.0782(2)	0.0769(8)	0.4452(2)	0.4481(8)
07	−0.1594(2)	−0.1587(9)	0.3515(2)	0.3517(9)

[a] *I*4/*m*; $a = b = 15.6731$ Å, $c = 3.8166$ Å, Ref. (*64*).
[b] Estimated standard deviations in the last place are given in parentheses.

work of Zachariasen (*114*, *115*) in 1948 and Mooney (*116*) in 1949, although positions for the halogen atoms had been postulated from geometrical considerations. Uranium and chlorine positions, but not oxygen locations, had been found in X-ray powder studies of uranyl chloride and its hydrates by Debets (*117*). The structure of UF_6 was solved by single-crystal X-ray diffraction in 1958 (*118*) but the U–F distances were not well defined. The $UOCl_2$ structure was said to be isomorphous with $PaOCl_2$ (*119*) although atomic coordinates had not been established for the former, and the UBr_4 structure had resisted solution for 18 years.

Mixed metal oxides have also received much attention and in a single publication, Loopstra and Rietveld (*75*) presented profile refinements of the structures of $CaUO_4$, $SrUO_4$, $BaUO_4$, Ca_2UO_5, Sr_2UO_5, Ca_3UO_6, and Sr_3UO_6. From this range of uranium studies, we select two experiments to illustrate the scope of the powder method; the UF_6 problem described below and the solution of the UBr_4 structure discussed in Section 4.2.2.

4.2.1. MoF_6, WF_6, and UF_6. UF_6 is a highly volatile, corrosive, and moisture sensitive material of central importance in the nuclear power industry. Diffraction studies on UF_6 at room temperature are difficult because the crystals sublime and recrystallize in slight temperature gradients. When contained, UF_6 is crystalline at room temperature; it has a vapor pressure of 15 kPa at 298°K, and a melting point of 337°K. The room temperature crystal structure was solved by Hoard and Stroupe in 1958 (*118*) from X-ray single-crystal photographs. The orthorhombic unit cell describes an array of interlocking UF_6 molecules but it was not clear from the X-ray study whether the UF_6 octahedron departed from regularity.

A preliminary study at room temperature (*28*) by powder neutron diffraction was subject to systematic errors from preferred orientation, the latter arising as the sample sublimed and recrystallized during the course of the experiment. In a profile analysis of data collected at 193°K (where the vapor pressure is reduced to approximately 0.2 Pa) the standard deviations of the positional parameters improved by a factor of 3 (*25*). This underlines the importance of being able to change temperature with ease. The results of the low-tem-

TABLE III

OBSERVED BOND DISTANCES IN THE ORTHORHOMBIC HEXAFLUORIDES MoF_6, WF_6, AND UF_6[a]

Bond	Neutron profile MoF_6, 193°K (Å) (*23*)	Neutron profile WF_6, 193°K (Å) (*24*)	Neutron profile UF_6, 193°K (Å) (*25*)	UF_6, 293°K single-crystal neutron (Å) (*120*)
M–F(1)	1.827(17)	1.838(15)	1.953(10)	1.981(4)
M–F(2)	1.861(29)	1.794(25)	2.026(21)	1.989(4)
M–F(3) (×2)	1.766(12)	1.800(10)	1.967(7)	1.978(3)
M–F(4) (×2)	1.817(20)	1.837(16)	1.983(14)	1.978(3)
Mean	1.809	1.818	1.902	1.980

[a] In the single-crystal neutron study 475 independent structure factors were utilized, and 12 positional and 24 thermal parameters were varied. In the profile studies, 12 positional and 1 thermal parameter were varied.

perature powder study are in good agreement with a recent single-crystal neutron diffraction study at 293°K (*120*). The structure of UF_6 does not change on cooling to 193°K; at both 293 and 193°K, the UF_6 molecule is a regular octahedron.

On the basis of similarities in X-ray photographs, the transition metal hexafluorides MoF_6 and WF_6 have been assigned an orthorhombic UF_6-type structure below 263.4 and 264.5°K, respectively (*121*). Above these temperatures they transform to a cubic, plastically crystalline phase. Neutron diffraction profile studies have been performed on the orthorhombic phases of MoF_6 (*23*) and WF_6 (*24*) at 193°K and confirm the UF_6-type structure. Results of the four neutron diffraction studies on orthorhombic hexafluorides are given in Table III. The structures of plastic phases of MoF_6 and WF_6 have also been refined (*26*, *27*) using a Kubic Harmonic function to describe the disorder of the MF_6 molecules.

4.2.2. Uranium tetrabromide. The UBr_4 structure has recently been solved (*22*) by a combination of powder studies by X-ray and neutron diffraction. The X-ray powder pattern of UBr_4 was published in 1957 (*122*) and indexed with the help of single-crystal photographs. The compound is monoclinic with space group $C2/m$ and four molecules per cell with $a = 10.92(2)$, $b = 8.69(3)$, $c = 7.05(1)$ Å, and $\beta = 93.9(1)°$. The structure remained unsolved from that date because good single crystals of the moisture sensitive substance could not be prepared.

Taylor and Wilson (*22*) located the uranium atoms at (0.20, 0, 0.40) by inspection of the X-ray intensities of Ref. (*122*), and deduced a trial structure by double bromine-bridging of every short U–U contact in such a way as to form a pentagonal bipyramid of bromine atoms around uranium. The model refined with the neutron profile technique to $R = 0.15$.

This new type of structure is shown in Fig. 4. The pentagonal bipyramids are edge-fused by Br(3) into chains parallel to b, and the chains are cross-linked into sheets parallel to (001) through a dual function atom Br(1) which is an apical bromine in one bipyramid and an equatorial bromine in an adjacent chain. The other

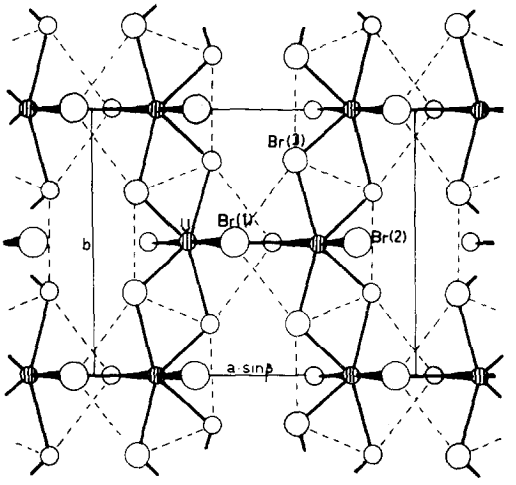

FIG. 4. A view of the UBr_4 structure down the c-axis. Uranium, hatched circles; bromine, open circles (*22*).

apical bromine atoms, Br(2), are terminal. The U–Br(3) distances are 2.85(2) and 2.93(2) Å, the U–Br(1) distances 2.78(3) Å (apical) and 2.95(2) Å (equatorial), and the U–Br(2) distance is 2.61(4) Å. UBr_4 appears to be the only actinide tetrahalide with a uranium coordination number of less than 8.

4.3. The Structures of Metal Hydrides

The power of neutron diffraction in the location of light atoms is most strikingly illustrated by the numerous studies on binary metal hydrides. Because of the complex phase relationships in many hydride systems, single crystals of specific phases are often difficult to prepare and powder measurements have played an important role in the elucidation of hydride structures. A typical example is a recent study (*102*) of hydrides of the alloys, RCo_5 (R = rare earth.)

The intermetallic compounds RCo_5 have been extensively researched in recent years because of their potential uses as permanent magnets and for hydrogen storage. Absorption and desorption of hydrogen takes place rapidly at room temperature, the equilibrium pressure being a few atmospheres (*123*). In the various RCo_5 systems, there are several hydrides whose structures are closely related. Kuijpers and Loopstra (*102*) reported a powder neutron diffraction study of hydrides with R = La, Ce, Pr, and Nd. Deuterides were preferred to hydrides because of the superior coherent neutron scattering properties of deuterium.

The RCo_5 intermetallics adopt the hexagonal $CaCu_5$-type structure in which there are alternating layers containing (R + 2Co) and (3Co) atoms, respectively (*124*). Preliminary X-ray diffraction studies showed that absorption of hydrogen is accompanied by an anisotropic expansion of the basal plane, leading to orthorhombic hydride structures. The expansion along the c-axis is relatively small. Profile analysis of neutron data on the β^{I}-, β^{II}-, and β^{III}-type structures, as found in $PrCo_5D_{3.6}$, $PrCo_5D_{2.9}$, and $CeCo_5D_{2.55}$, respectively, showed that deuterium atoms occupy both octahedral and tetrahedral interstices. In the β^{I} hydride, the occupancy numbers of these sites are approximately equal. The limiting composition is RCo_5D_4 and the space group is *Cmmm*. The patterns of the β^{II}-type compounds could only be indexed on an orthorhombic body-centered cell which is doubled along the c-axis. The space group for the β^{II} type is *Im2m*. The occupancy of the octahedral sites is reduced compared with that in $PrCo_5D_{3.6}$ and the vacancies lead to appreciable ordered shifts of the metal atoms. In the β^{III} phase, the cell is again doubled along the c-axis and the superstructure cell is C-centered. One of the octahedral sites is now empty, giving rise to a limiting composition of RCo_5D_3. The β^{I} and β^{III} types represent phases for which ideal stoichiometries can be achieved. The β^{II} structure is an intermediate between β^{I} and β^{III} but it has an ideal stoichiometry which lies well outside its range of existence. This complex interplay between order and disorder at room temperature is typical of metal hydrides and arises because the defect interaction energies are much lower than those in ionic materials.

Many other examples of light atom problems are cited in Table I.

4.4 The Determination of Atomic Distributions

One of the most valuable properties of the neutron is the variation of the coherent scattering amplitude between adjacent elements in the periodic table, contrasting markedly with the smooth dependence of X-ray scattering factors upon atomic number (Fig. 1). These variations often allow neighboring elements to be distinguished crystallographically. Typical examples are the scattering amplitudes of nitrogen (0.94) and oxygen (0.577), magnesium (0.532) and aluminium (0.345), and iron (0.96) and cobalt (0.25). Of particular importance are those elements whose scattering amplitudes are negative; hydrogen (–0.378), lithium (–0.214), titanium (–0.34), vanadium (–0.051), and manganese (–0.387). For these nuclei there is no change of phase on scattering.

Von Dreele and Cheetham (*54*) have recently exploited the negative scattering length of titanium in determining the extent of cation ordering in $TiNb_2O_7$ and orthorhombic $Ti_2Nb_{10}O_{29}$. The idealized structure of $TiNb_2O_7$ is shown in Fig. 5. It is a block-type struc-

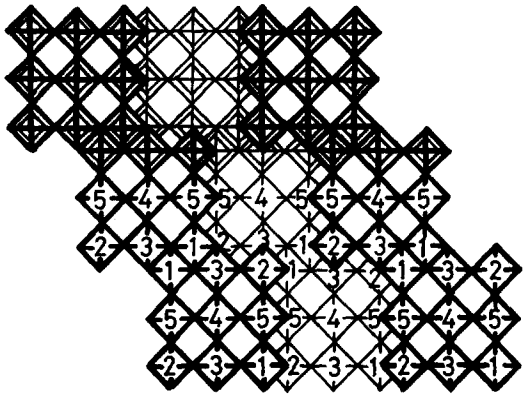

FIG. 5. The idealized structure of $TiNb_2O_7$. MO_6 octahedra with thick and thin outlines have M at $z = 0$ and $z = \frac{1}{2}$, respectively. Metal sites $M(1)$ to $M(5)$ are labeled (*54*).

ture (see Sect. 4.1) containing columns of ReO_3, 3×3 octahedra in cross section, but linked in a different manner to $GeO_2 \cdot 9Nb_2O_5$. Single-crystal X-ray studies by Wadsley (*125*) on these titanium–niobium oxides indicated a random distribution of Ti and Nb over the different metal sites. The powder neutron diffraction studies, however, reveal extensive ordering in $TiNb_2O_7$, with a distribution of titanium consistent with the site potentials calculated on an ionic model (Table IV). A similar result was obtained for ortho-$Ti_2Nb_{10}O_{29}$. The final observed and calculated profile for $TiNb_2O_7$ is shown in Fig. 6. The significance of this work is that it deals for the first time with the extent and origin of cation ordering in a mixed transition metal oxide of this type. In addition, ortho-$Ti_2Nb_{10}O_{29}$ represents the most complex structure studied to date by profile analysis, with 41 positional parameters and six occupancy numbers.

In another recent publication, Armytage and Fender (*110*) used powder neutron profile analysis to examine TaON. This compound has a ZrO_2-type structure and the neutron measurements establish that the oxygen and nitrogen ions are fully ordered, again in a manner consistent with site potential calculations. A short nitrogen–nitrogen contact distance is also observed.

For many years, neutron diffraction has afforded the only possible method for determining atomic distributions in many compounds. The advent of profile analysis is now extending the range of such studies to more complex materials and important applications to nonstoichiometric compounds, alloys, and minerals are anticipated.

4.5. *Phase Transitions*

The facility with which powder neutron diffraction measurements may be made over a wide range of temperatures, already emphasized in Section 2.2, makes the powder method an attractive means of investigating phase transitions. Indeed, the use of polycrystalline samples is obligatory in cases where single crystals disintegrate on passing through the transition. Consequently, powders have already played an important role in the study of

TABLE IV

CATION DISTRIBUTION AND SITE POTENTIALS IN $TiNb_2O_7$ (*54*)[a]

Metal site	Titanium concentration (%)[b]	Average site charge	Site potential (obs dist.)/Å^{-1}	Site potential (random dist.)/Å^{-1}
*M*1	33.8(1.1)	+4.66	−3.25	−3.20
*M*2	64.5(1.3)	+4.35	−3.16	−3.19
*M*3	26.0(1.3)	+4.74	−3.44	−3.35
*M*4	14.0(1.9)	+4.86	−3.99	−4.04
*M*5	20.6(1.4)	+4.79	−3.56	−3.59

[a] Coulombic lattice energy for (i) observed distribution = 51 364 kJ/mole, (ii) random distribution = 51 230 kJ/mole.

[b] Estimated standard deviations in parentheses.

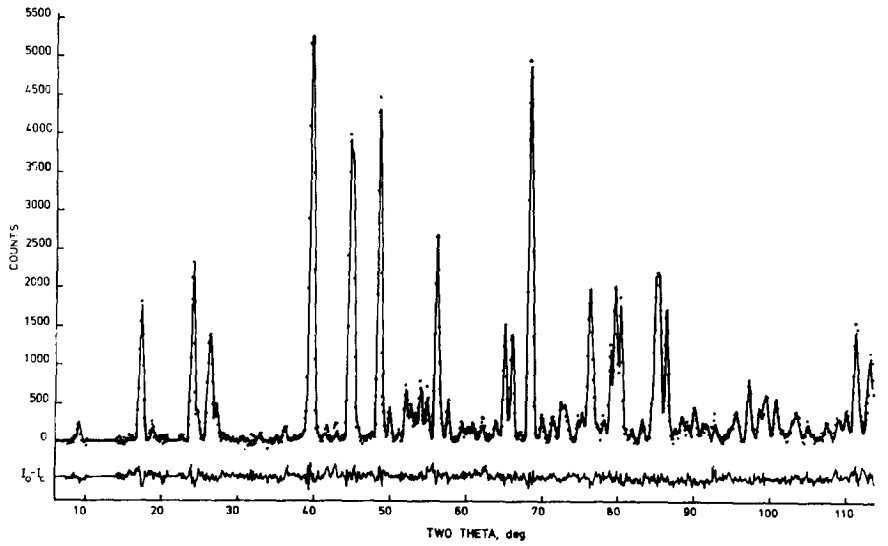

FIG. 6. Observed (dots) and calculated (smooth curve) neutron diffraction profile of $TiNb_2O_7$. A difference curve is also shown. Six hundred and three allowed reflections contribute to the profile (*54*).

order–disorder phenomena and ferroelectric transitions. Because it has a magnetic moment, the neutron is also an excellent probe for detailed investigations of magnetically ordered materials. Magnetic ordering is primarily a low-temperature phenomenon so that powders are normally used for studies of this type; several examples incorporating profile analysis are cited in Table I. Neutron diffraction measurements on magnetic systems have, however, been reviewed elsewhere (*126*) so in the present work we prefer to describe some recent measurements on ferroelectric materials.

The ferroelectric $KNbO_3$ has been examined (*66*) by powder neutron diffraction at 543°K (tetragonal phase), 295°K (orthorhombic phase), and 230°K (rhombohedral phase). Hewat reports that profile analysis of the data provides information which is probably more accurate than that obtained by single-crystal methods, with shorter counting times. Refinements were carried out with both isotropic and anisotropic temperature factors. The powder results on the tetragonal phase are compared with the single-crystal results in Table V. In all three phases, the magnitudes and directions of the atomic displacements account for the observed changes in the spontaneous polarization of $KNbO_3$; the effective ionic charges were estimated from infrared and dielectric data.

The antiferroelectric ammonium dihydrogen phosphate has also been examined and is a system in which single crystals break up on cooling through the transition. Powder neutron diffraction measurements (*103*) above and below the transition at 245°K show that in the paraelectric phase, the hydrogen atoms associated with the phosphate group are disordered over two possible sites; in the antiferroelectric phase only one of these sites is occupied. The dipole moments associated with each $H_2PO_4^-$ group cancel out so that there is no net dipole, a situation which contrasts with the ferroelectric behavior of KH_2PO_4 (*127*).

4.6. High-Resolution Electron Microscopy and Profile Analysis

The development of profile analysis has taken place simultaneously with some rapid changes in the field of electron microscopy. Lattice images with a resolution of 3.5 Å can now be obtained from crystals of approximately 100 Å thickness (*128*). Powder specimens are normally sufficient for this purpose. It has been shown (*129*, *130*) that two-dimensional lattice images of thin crystals, under proper imaging conditions, represent ap-

TABLE V

POWDER RESULTS FOR THE TETRAGONAL $KNbO_3$ PHASE AT 270°C COMPARED WITH THOSE FOR THE SINGLE-CRYSTAL EXPERIMENT (*66*)[a]

	Single-crystal, neutron $\lambda = 1.143$ Å	Powder, neutron $\lambda = 1.0332$ Å							
		Isotropic $B(\kappa)$			Anisotropic $B_{jj}(\kappa)$				Unit
Δ_z (K)	0.023 ± 10	0.018 ± 3			0.018 ± 6				cÅ
Δ_z (Nb)	0.0	0.0			0.0				cÅ
Δ_z (O_I)	0.040 ± 3	0.040 ± 1			0.044 ± 1				cÅ
Δ_z (O_{II})	0.042 ± 3	0.041 ± 1			0.040 ± 1				cÅ
$= \Delta_z$ (O_{III})	0.042 ± 3	0.041 ± 1			0.040 ± 1				cÅ
	B_{11}	B_{22}	B_{33}	$B(\kappa)$	B_{11}	B_{22}	B_{33}	$\bar{B}_{jj}(\kappa)$	
B_{jj} (K)	1.66 ± 39	1.66	1.18 ± 47	1.16 ± 5	1.04 ± 16	1.04	1.26 ± 26	1.11	Å²
B_{jj} (Nb)	0.79 ± 16	0.79	0.24 ± 16	0.55 ± 3	0.67 ± 6	0.67	0.31 ± 16	0.55	Å²
B_{jj} (O_I)	0.95 ± 24	0.95	1.26 ± 47	1.06 ± 7	1.18 ± 10	1.18	0.58 ± 21	0.98	Å²
B_{jj} (O_{II})	0.87 ± 24	0.79 ± 8	1.26 ± 45	0.73 ± 4	0.99 ± 10	0.45 ± 6	1.00 ± 10	0.81	Å²
B_{jj} (O_{III})	0.79	0.87	1.26	0.73	0.45	0.99	1.00	0.81	Å²
c/a		1.0165		1.01685 ± 35		1.01687 ± 35			

[a] The $\Delta_z(\kappa)$ are the atomic displacements from the aristotype positions in fractions of the cell edge $c = 4.063$ Å, the Debye–Waller temperature factors $B_{jj}(\kappa) = 8\pi^2\langle U_{jj}(\kappa)^2\rangle$.

proximately the projected charge density in the crystal. The contrast in the image is therefore dominated by contributions from any heavy elements present. In materials where the projection of the heavy atom positions can be interpreted with confidence, this method provides a possible route to a trial structure for subsequent profile analysis.

A complete structure determination by a combination of high-resolution electron microscopy and powder neutron diffraction has recently been reported by Jacobson and Hutchison (*63*). They examined the structure of perovskite-related 12-layer $BaCoO_{2.6}$. The lattice images show sheets of Ba atoms, projected edge-on along $\langle 10\bar{1}0\rangle$, as dark lines. The slope of the lines distinguishes cubic (*c*) from hexagonal (*h*) close-packed BaO_3 layers. Of the 42 possibilities for 12-layer stacking, the previously unknown sequence $(ccchhh)_2$ gave the best correlation with the lattice image. This was used as the basis for a starting model for refinement of the powder neutron diffraction data. Preliminary refinements confirmed the *ccchhh* sequence, but indicated that the central cubic layer had the composition BaO_2. With this model, 22 structural parameters, including oxygen occupancy numbers, were refined. The composition from the final profile refinement was $BaCoO_{2.60(7)}$, in good agreement with the chemical analysis. For structure types which give readily identifiable lattice images, for example the niobium oxides, this combination of diffraction techniques provides a useful means of determining the structure using only polycrystalline samples.

5. Future Developments and Limitations

We now consider some current and future developments in the use of profile analysis and examine the limitations of the method. We believe that the case for using profile analysis to determine atomic coordinates in moderately complex systems is now proven. Here we discuss the limits of profile analysis in terms of the size of the crystallographic problem and consider how its scope might be further increased. The reliability with which temperature factors can be determined is debatable and this is also discussed. Finally, we assess the use of profile analysis with X radiation and pulsed neutron sources.

Before dealing with these topics, however, a word of caution is necessary for those who intend to use profile analysis. In our experience, the R_p-factor rarely falls to the value expected on the basis of counting statistics. The pri-

mary causes of this are errors in the background estimation (Sect. 5.4) and the breakdown of the assumption that the peaks are Gaussian in shape. As a result, two common problems may arise; it is sometimes difficult to know when the refinement procedure is complete, and it is often hard to distinguish between alternative models. To a large extent, these questions are presently answered by intuition and it is likely that this state of affairs will continue. The Hamilton significance tests, which might normally be used to tackle the second problem, are unfortunately unreliable because of the presence of the systematic errors mentioned above. We do, however, recommend the calculation of a difference Fourier map (Sect. 5.3) based upon the final model so that serious errors in the structure are avoided.

5.1. Limits of Profile Analysis and Instrumental Resolution

Although profile analysis dispenses with the need to completely resolve overlapping reflections, instrumental resolution is an important factor in revealing some of the structure associated with overlap. In the hypothetical limit where each reflection is a δ-function, all reflections which do not overlap exactly can be measured independently by the powder method. In reality, our resolution is limited by the need to carry out experiments in a reasonable length of time (the resolution can only be improved at the expense of the incident beam intensity) and by line broadening arising from the particle size effect (*131*). Hewat (*132*) has recently designed a neutron powder diffractometer which gives the optimum resolution permitted by these limits. High resolution is achieved by increasing the take-off angle at the monochromator beyond 90° and by choosing a suitable combination of monochromator mosaic spread and collimator divergencies. At the same time, the effective intensity is increased by the deployment of multiple counter banks. Hewat estimates that with such an instrument it would be possible to refine low-symmetry structures up to a unit cell limit of 3500 Å^3. The largest unit cell refined to date, 2177 Å^3, is that of $Ti_2Nb_{10}O_{29}$ (*54*).

With a hypothetical instrument in which the resolution (0.1° at 90° 2θ) is limited only by the particle size effect, adjacent reflections from a primitive cubic cell with $a_0 = 24$ Å can just be resolved. Thus, with a wavelength of 1.5 Å, a maximum of 640 intensities could be collected in the range $0° < 2\theta < 120°$ (the angular range typically available on most instruments). With a 3:1 ratio of reflections to variables, this would allow the determination of up to approximately 213 variables. The number would be about the same for systems of lower symmetry. The equivalent calculation for existing high-resolution instruments (resolution ~0.3° at 90° 2θ) indicates a limit of approximately 75 variables at the present time.

It is more difficult to estimate the optimum combination of flux and resolution to suit a particular problem. This is illustrated in a recent study of lanthanum and cerium trifluorides (*15*). The LaF_3 data were collected in 6 hr on the low-resolution D2 diffractometer at the ILL, Grenoble, up to a maximum 2θ value of 60°. Data collection for the isostructural CeF_3 took 85 hr on the high-resolution D1A instrument at ILL, with a maximum 2θ of 115°. The results of these experiments (Table VI) show that despite the marked increase in resolution, the precision of the structural parameters for CeF_3 is superior by less

TABLE VI

ATOMIC COORDINATES AND THERMAL PARAMETERS FROM PROFILE ANALYSIS OF NEUTRON DATA ON LaF_3 (LOW RESOLUTION) AND CeF_3 (HIGH RESOLUTION) (*15*)[a]

Atom		LaF_3	CeF_3
La/Ce:	x	0.6609(10)	0.6607(7)
	B (Å^2)	0.24(6)	0.29(5)
F(1):	x	0.3667(6)	0.3659(3)
	y	0.0540(4)	0.0540(2)
	z	0.0824(5)	0.0824(4)
	B (Å^2)	0.70(5)	1.17(3)
F(2):	z	0.1855(9)	0.1871(5)
	B (Å^2)	0.70(5)	1.01(6)
F(3):	B (Å^2)	0.70(5)	1.60(15)

[a] Space group $P\bar{3}c1$; LaF_3: $a = 7.185$, $c = 7.351$ Å; CeF_3: $a = 7.131$, $c = 7.286$ Å; 6 Ln in (f)... $x\,0\,\frac{1}{4}$; 12F(1) in (g)... $x\,y\,z$; 4F(2) in (d)... $\frac{1}{3}\,\frac{2}{3}\,z$; 2F(3) in ($a$)... $0\,0\,\frac{1}{4}$.

than a factor of 2. For relatively simple structures of this type, a high-flux, low-resolution instrument is clearly adequate. However, good resolution is certainly necessary when refining more complex structures with a large number of variables. At the present time, the choice of instrument for a particular experiment is based upon experience rather than calculation.

The multiple counter banks proposed for Hewat's high-resolution diffractometer have now been installed on several diffractometers at Harwell and Grenoble. The problem of combining the data sets from different counters has been solved, but the large vertical acceptance angle on some of the instruments has increased the distortion of the peak shape which is apparent on all instruments at low angles. The corrections which are necessary for profile calculations have been discussed by Cooper and Sayer (*133*).

5.2. Constrained Refinements

The original Rietveld program permits the introduction of a limited number of linear and quadratic constraints between atomic coordinates, occupancy numbers, or thermal parameters. These constraints may be required by the space group symmetry, or they may be used to reduce the number of variables, for example, in a molecular crystal where the geometry of some part of the molecule may already be known. Clarke, at Oxford, has now extended the capacity of the program in this direction by introducing flexible constraints of the type described by Waser (*134*). The subsidiary conditions, suitable weighted, are treated as observational equations. This is applicable in cases where the geometry of a molecular fragment is approximately known, and it is hoped that the Clarke Program will increase the range of molecular crystals which come within the scope of profile analysis.

5.3. Fourier Analysis

The limitations of powders for the ab initio solution of structures have already been discussed in Sections 2 and 4. The main difficulty is that the Fourier inversion of a powder pattern gives only a radial distribution function rather than the three-dimensional Patterson map obtained from single-crystal data. A rather useful Fourier method is possible, however, with profile analysis if most of the atoms in the unit cell have been located. The standard output from a Rietveld least-squares refinement includes a list of observed and calculated integrated intensities (I_k's) for individual reflections. The calculated I_k's are determined by the structural model. The observed I_k's are obtained by multiplying I_k (calc) by the average ratio $Y_i(\text{obs})/Y_i(\text{calc})$ for points i within the range of influence of the reflection. Although this is clearly not rigorous, it does serve as a basis from which three-dimensional Fourier maps may be calculated. It can also be used to estimate a conventional R-factor based upon structure factors or integrated intensities.

A Fourier map calculated in this manner has recently been used to determine the structure of deuterium β-alumina (*42*). The structure was initially refined with only aluminium and oxygen atoms, the starting coordinates being taken from the structure of sodium β-alumina. The deuterium positions were then located in the Fourier map (Fig. 7). The deuterium positions are different from those of the metal ions in sodium and silver β-alumina.

This procedure should be used cautiously but it is certainly useful in cases where most of the structure has been determined.

5.4. Thermal Parameters and the Background Correction

Powder neutron diffraction data is routinely collected at 4.2°K (Sect. 2.2) and consequently, an overall temperature factor usually affords an adequate description of the thermal motion. For room temperature data on metal oxides, halides, etc., independent isotropic B-factors for cations and anions, respectively, will usually suffice. However, in materials where the bonding is markedly anisotropic, a more sophisticated description of the thermal motion is required. This is perhaps why profile analysis has not yet been extensively applied to organic materials. Facilities for refining anisotropic temperature factors are widely available in modifications of the Rietveld program and anisotropic refinements have been carried out

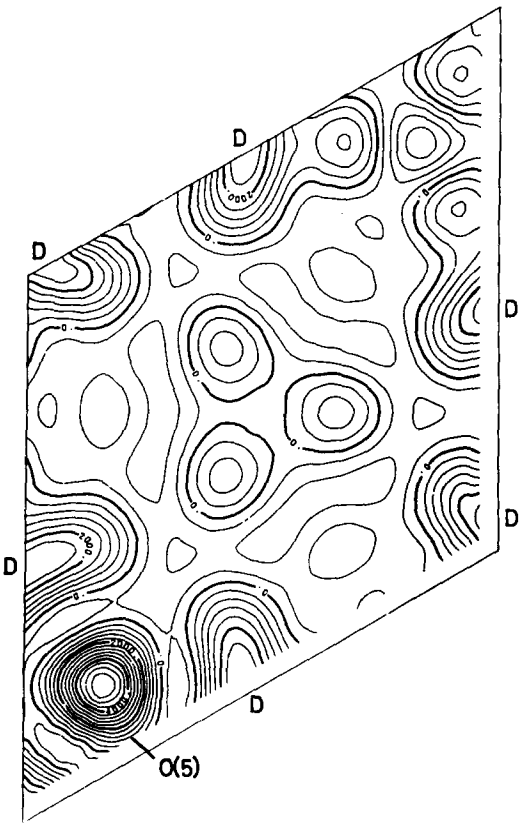

FIG. 7. Fourier map of the mirror plane of deuterium β-alumina at 4.5°K. The deuterium positions (D) and the mid-oxygen position (05) are labeled (*42*).

successfully on ferroelectric materials (Sect. 4.5). Nevertheless, in our opinion there is still doubt as to whether the thermal parameters derived from profile refinements are, in general, reliable. In the refinements of LaF_3 and CeF_3, for example, widely different temperature factors for fluorine were obtained from data collected on different instruments although the atomic coordinates are strikingly similar (Table VI). This uncertainty probably arises because of the restricted range of $\sin\theta/\lambda$ over which data is normally collected and, in particular, the manner in which the background correction is made.

The subtraction of the background is normally carried out prior to the least-squares calculation. The background level is estimated at relatively clear portions of the diffraction pattern. At high scattering angles, as the density of reflections increases (with a maximum at 90° 2θ) and the instrumental resolution deteriorates, the diffraction pattern may not reach the true background level. The background can then only be estimated by extrapolating from clear regions of the pattern at low angles. This problem is very noticeable on low-resolution instruments and can, of course, lead to systematic errors in the Debye–Waller factors.

Sabine and Clarke (*135*) have recently modified the profile program so that an estimation of the background is no longer necessary. The background is calculated by summing the instrumental background, the incoherent scattering due to isotopic disorder and nuclear spin effects, the paramagnetic scattering, and any diffuse scattering arising from random substitutional atomic defects. The least-squares refinement then compares the *total* observed diffraction pattern with the calculated profile. The degree of substitutional disorder can also be refined. The program was used for a refinement of cosmochlore, $NaCrSi_2O_7$, in which there is substantial incoherent scattering from chromium. The calculation ignores thermal diffuse scattering (TDS) so it is suitable primarily for low-temperature data. At the present time, the inclusion of first- and higher-order TDS effects is not possible.

An alternative method of minimizing errors due to the background correction is to collect the diffracted neutrons via an analyzing crystal. This should be set to reflect only elastically scattered neutrons. The removal of inelastically scattered neutrons considerably enhances the peak-to-background ratio and reduces the background level. The disadvantage of this approach is that it greatly increases the counting time.

5.5. *Profile Analysis of X-ray Data*

The success of neutron profile analysis has naturally stimulated an interest in the possibility of carrying out profile refinements of X-ray powder data. The main difficulty in adapting the method for X-rays has been the description of the peak shape which is not normally Gaussian. In addition, of course, X-ray patterns usually contain less informa-

tion than neutron patterns because of the dependence of X-ray scattering factors upon angle. Nevertheless, since X-ray facilities are less expensive and more widely available than neutron sources, X-ray profile analysis is an important area in which rapid growth can be anticipated.

In a recent publication, Malmros and Thomas (*136*) report an adaptation of the Rietveld program to handle X-ray intensity data from microdensitometer measurements of Guinier–Hägg powder films. The advantages of the focusing camera over the powder diffractometer are better resolution, the complete exclusion of $K\alpha_2$ contributions, and the reduction of preferred orientation by the transmission geometry and sample rotation. They found that the peak shape was adequately described by a modified Lorentz function although a parameter was necessary to correct for asymmetry. In a pilot investigation, an X-ray profile analysis of α-Bi_2O_3 was compared with a modest single-crystal X-ray study (*137*). The results are summarized in Table VII, which also includes the values obtained in a recent powder neutron diffraction refinement (*50*). The standard deviations from the X-ray powder study are two to three times larger than those from the single-crystal experiment. The neutron refinement is inferior to the latter with respect to bismuth positions but superior in the location of oxygen.

Programs for carrying out profile analysis of X-ray powder data have also been reported by Taylor and Cox (*8*) and Mackie and Young (*138*). In the former instance, the Busing–Martin–Levy least-squares program (*6*) was modified. The reflection half-widths are predetermined by direct measurement and the unit cell dimensions are obtained in a preliminary analysis of the line positions. Mackie and Young give no details of their program.

TABLE VII

A COMPARISON OF ATOMIC COORDINATES[a] FOR α-Bi_2O_3[b]

Atom		x	y	z
Bi(1)	a	0.5240(1)	0.1831(1)	0.3613(1)
	b	0.5254(7)	0.1825(5)	0.3608(5)
	c	0.5227(5)	0.1835(4)	0.3592(3)
Bi(2)	a	0.0409(2)	0.0425(1)	0.7762(1)
	b	0.0431(6)	0.0416(5)	0.7777(5)
	c	0.0428(4)	0.0425(4)	0.7766(3)
O(1)	a	0.780(4)	0.300(3)	0.710(3)
	b	0.767(7)	0.304(5)	0.711(6)
	c	0.7782(6)	0.3048(4)	0.7080(5)
O(2)	a	0.242(5)	0.044(4)	0.134(4)
	b	0.262(8)	0.062(5)	0.144(6)
	c	0.2332(7)	0.0465(5)	0.1287(5)
O(3)	a	0.271(4)	0.024(3)	0.513(3)
	b	0.305(8)	0.026(6)	0.510(7)
	c	0.2669(6)	0.0290(5)	0.5090(5)

[a] Estimated standard deviations in last place are given in parentheses.

[b] From (*a*) single-crystal X-ray study (*137*); (*b*) profile refinement of X-ray powder data (*136*); (*c*) profile refinement of neutron powder data (*50*). Space group $P2_1/c$; $a = 5.8478$, $b = 8.1673$, $c = 7.5102$ Å, $\beta = 112.98°$.

5.6. *Pulsed Neutron Sources*

The present generation of high-flux beam reactors represents the limit of what is economically feasible within our existing technology and consequently, there is now considerable interest in the development of pulsed neutron sources as alternatives to the steady-state reactor. Two types of facility are currently being assessed: the LINAC in which neutrons are generated when short pulses of electrons are fired into a gold/uranium target, and the spallation source in which neutrons are produced by proton spallation of a ^{238}U target. The pulsed sources characteristically produce a white beam with a high flux of short wavelength neutrons, so that diffraction data can be collected out to very high values of the scattering vector.

The diffraction pattern is recorded by time-of-flight (TOF) methods using a counter at a fixed scattering angle. The resulting powder pattern contains the scattered intensity as a function of increasing d-spacing. Maier–Leibnitz and Springer (*139*) have shown that under these conditions, the optimum resolution may be achieved by placing a detector in the back-scattering position (Fig. 8). Recent measurements (*140*) have confirmed this prediction. Decker and co-workers (*104*) have

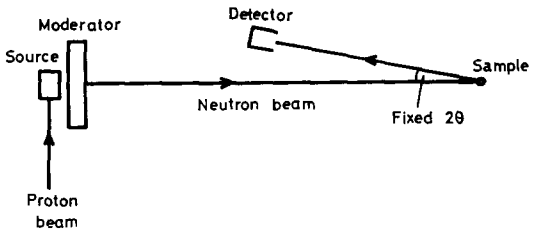

FIG. 8. Schematic layout of a back-scattering, time-of-flight spectrometer.

written a computer program for profile analysis of TOF powder data. The main differences between this program and the Rietveld program are the inclusion of the λ^4 dependence of the TOF powder intensities and the use of a three-parameter function to fit the background. Independently, Windsor and Sinclair (*95*) have recently modified the Rietveld program to handle TOF data. With some simple changes, these programs could also be adapted to handle variable-λ, fixed-θ X-ray powder data collected on a synchroton radiation source.

A spallation source giving a neutron flux of approximately 3×10^{16} neutrons sec^{-1} is quite feasible with protons from a high-intensity cyclotron. Extrapolating the performance of a pilot project on ZING-P at the Argonne National Laboratory suggests that on such a facility, a high-resolution powder pattern could be collected in approximately 1 sec! This exciting prospect would open up a whole new range of possibilities for neutron diffraction in which profile analysis would play an important role.

Acknowledgment

We are grateful to Professor J. S. Anderson, F.R.S., who suggested that this review should be written.

References

1. H. M. RIETVELD, *Acta Crystallogr.* **22**, 151 (1967).
2. H. M. RIETVELD, *J. Appl. Cryst.* **2**, 65 (1969).
3. G. E. BACON, "Neutron Diffraction," 3rd ed., Oxford Univ. Press, London/New York (1975).
4. A. K. CHEETHAM, B. E. F. FENDER, AND R. I. TAYLOR, *J. Phys. C.* **4**, 2160 (1971).
5. C. J. CARLILE AND D. C. SALTER, High Pressure Techniques for Thermal Neutron Scattering Experiments, Rutherford Laboratory Report: RL-75-096 (1975).
6. W. R. BUSING, K. O. MARTIN, AND H. A. LEVY, USAEC Report ORNL-TM-305 (1962).
7. W. C. HAMILTON AND J. A. IBERS, *Acta Crystallogr.* **16**, 1209 (1963).
8. J. C. TAYLOR AND G. W. COX, AAEC/E257 (1973).
9. H. M. RIETVELD, *Acta Crystallogr.* **20**, 508 (1966)
10. B. O. LOOPSTRA AND H. M. RIETVELD, *Acta Crystallogr. B* **25**, 1420 (1969).
11. P. FISCHER, W. HÄLG, D. SCHWARZENBACH, AND H. GAMSJÄGER, *J. Phys. Chem. Solids* **35**, 1683 (1974).
12. J. C. TAYLOR AND P. W. WILSON, *J. Less-Common Metals* **34**, 257 (1974).
13. A. J. JACOBSON, L. MCBRIDE, AND B. E. F. FENDER, *J. Phys. C.* **7**, 783 (1974).
14. A. K. CHEETHAM AND N. NORMAN, *Acta Chem. Scand. A* **28**, 55 (1974).
15. A. K. CHEETHAM, B. E. F. FENDER, H. FUESS, AND A. F. WRIGHT, *Acta Crystallogr. B* **32**, 94 (1976).
16. N. W. ALCOCK AND H. D. B. JENKINS, *J. Chem. Soc. Dalton*, 1907 (1974).
17. J. C. TAYLOR AND P. W. WILSON, *Acta Crystallogr. B* **30**, 2803 (1974).
18. J. H. LEVY, J. C. TAYLOR, AND P. W. WILSON, *J. Less-Common Metals* **39**, 265 (1975).
19. J. H. LEVY, J. C. TAYLOR, AND P. W. WILSON, *Acta Crystallogr. B* **31**, 880 (1975).
20. J. C. TAYLOR AND P. W. WILSON, *Acta Crystallogr. B* **29**, 1942 (1973).
21. J. C. TAYLOR AND P. W. WILSON, *Chem. Commun.* 598 (1974).
22. J. C. TAYLOR AND P. W. WILSON, *Acta Crystallogr. B* **30**, 2664 (1974).
23. J. H. LEVY, J. C. TAYLOR, AND P. W. WILSON, *Acta Crystallogr. B* **31**, 398 (1975).
24. J. H. LEVY, J. C. TAYLOR, AND P. W. WILSON, *J. Solid State Chem.* **15**, 360 (1975).
25. J. C. TAYLOR AND P. W. WILSON, *J. Solid State Chem.* **14**, 378 (1975)
26. J. H. LEVY, P. L. SANGER, J. C. TAYLOR, AND P. W. WILSON, *Acta Crystallogr. B* **31**, 1065 (1975).
27. J. H. LEVY, J. C. TAYLOR, AND P. W. WILSON, *J. Less-Common Metals* **45**, 155 (1976).
28. J. C. TAYLOR, P. W. WILSON, AND J. W. KELLY, *Acta Crystallogr. B* **29**, 7 (1973).
29. J. C. TAYLOR AND P. W. WILSON, *Acta Crystallogr. B* **30**, 1216 (1974).
30. J. C. TAYLOR AND P. W. WILSON, *Acta Crystallogr. B* **30**, 1481 (1974).
31. M. T. HUTCHINGS, A. K. GREGSON, P. DAY, AND D. H. LEECH, *Solid State Commun.* **15**, 313 (1974).
32. B. O. LOOPSTRA, B. VAN LAAR, AND D. J. BREED, *Phys. Lett. A* **26**, 526 (1968).

33. C. J. J. Van Loon and J. De Jong, *Acta Crystallogr. B* **31**, 2549 (1975).
34. C. J. J. Van Loon and D. J. W. Ijdo, *Acta Crystallogr. B* **31**, 770 (1975).
35. A. L. M. Bongaarts and B. Van Laar, *Phys. Rev. B* **6**, 2669 (1972).
36. J. C. Taylor and P. W. Wilson, *J. Inorg. Nucl. Chem.* **36**, 1561 (1974).
37. H. T. Witteveen, D. L. Jongejan, and V. Brandwijk, *Mat. Res. Bull.* **9**, 345 (1974).
38. A. N. Christensen, T. Johansson, and S. Quézel, *Acta Chem. Scand. A* **28**, 1171 (1974).
39. J. C. Taylor and P. W. Wilson, *Acta Crystallogr. B* **30**, 175 (1974).
40. J. C. Taylor and P. W. Wilson, *Acta Crystallogr. B* **29**, 1073 (1973).
41. J. C. Taylor and P. W. Wilson, *Acta Crystallogr. B* **30**, 169 (1974).
42. W. A. England, A. J. Jacobson, and B. C. Tofield, *Chem. Commun.*, 895 (1976).
43. M. Pernet, J. C. Joubert, and C. Berthet-Colominas, *Sol. State Comm.* **17**, 1505 (1975).
44. M. Bonnet, A. Delapalme, and H. Fuess, *Acta Crystallogr. A* **31**, 264 (1975).
45. A. K. Cheetham and C. N. R. Rao, *Acta Crystallogr. B* **32**, 1579 (1976).
46. T. G. Worlton and R. A. Beyerlein, *Phys. Rev. B* **12**, 1899 (1975).
47. R. B. Von Dreele, L. Eyring, A. L. Bowman, and J. L. Yarnell, *Acta Crystallogr. B* **31**, 971 (1975).
48. J. X. Bourcherle and J. Schweizer, *Acta Crystallogr. B* **31**, 2745 (1975).
49. H. Fuess, G. Bassi, M. Bonnet, and A. Delapalme, *Solid State Commun.* **18**, 557 (1976).
50. C. E. Infante-Barros. Ph.D. Thesis, University of Oxford (1975).
51. B. O. Loopstra, *J. Appl. Crystallogr.* **3**, 94 (1970).
52. B. O. Loopstra, *Acta Crystallogr. B* **26**, 656 (1970).
53. J. C. Taylor and P. W. Wilson, *Acta Crystallogr. B* **30**, 151 (1974).
54. R. B. Von Dreele and A. K. Cheetham, *Proc. Roy. Soc. London A* **338**, 311 (1974).
55. A. W. Hewat, *Ferroelectrics* **6**, 215 (1974).
56. B. Van Laar and J. B. A. A. Elemans, *J. Phys.* **32**, 301 (1971).
57. A. J. Jacobson and A. W. J. Horrox, *Acta Crystallogr. B* **32**, 1003 (1976).
58. J. B. A. A. Elemans, B. Van Laar, K. R. Van Der Veen, and D. J. W. Ijdo, *J. Solid State Chem.* **3**, 590 (1971).
59. Z. Tomkowicz and B. Van Laar, *Phys. Status Solidi (a)*, **23**, 683 (1974).
60. A. J. Jacobson, *Acta Crystallogr. B* **32**, 1087 (1976).
61. A. J. Jacobson and B. E. F. Fender, *J. Phys. C.* **8**, 844 (1975).
62. C. Greaves, A. J. Jacobson, B. C. Tofield, and B. E. F. Fender, *Acta Crystallogr. B* **31**, 641 (1975).
63. A. J. Jacobson and J. L. Hutchison, *J. Chem. Soc. Chem. Commun.*, 116 (1976).
64. J. S. Anderson, D. J. M. Bevan, A. K. Cheetham, R. B. Von Dreele, J. L. Hutchison, and J. Strähle, *Proc. Roy. Soc. London A* **346**, 139 (1975).
65. A. W. Hewat, *Ferroelectrics*, **7**, 83 (1974).
66. A. W. Hewat, *J. Phys. C.* **6**, 2559 (1973).
67. M. Ahtee and A. W. Hewat, *Acta Crystallogr. A* **31**, 846 (1975).
68. H. Weitzel, *Acta Crystallogr. A* **32**, 592 (1976).
69. A. J. Jacobson, B. M. Collins, and B. E. F. Fender, *Acta Crystallogr. B* **30**, 1705 (1974).
70. A. J. Jacobson, B. M. Collins, and B. E. F. Fender, *Acta Crystallogr. B* **32**, 1083 (1976).
71. B. M. Collins, A. J. Jacobson, and B. E. F. Fender, *J. Solid State Chem.* **10**, 29 (1974).
72. A. J. Jacobson, B. M. Collins, and B. E. F. Fender, *Acta Crystallogr. B* **30**, 816 (1974).
73. G. Thornton and A. J. Jacobson, *Mat. Res. Bull.* **11**, 837 (1976).
74. D. E. Cox and A. W. Sleight, *Solid State Commun.* **19**, 969 (1976).
75. B. O. Loopstra and H. M. Rietveld, *Acta Crystallogr. B* **25**, 787 (1969).
76. W. Prandl, *Solid State Commun.* **11**, 645 (1972).
77. W. Prandl, *Phys. Status Solidi (b)* **55**, K159 (1973).
78. W. Prandl, *Solid State Commun.* **10**, 529 (1972).
79. K. Selte, A. Kjekshus, and A. F. Andresen, *Acta Chem. Scand.* **26**, 4057 (1972).
80. T. J. A. Popma, C. Haas, and B. Van Laar, *J. Phys. Chem. Solids* **32**, 581 (1971).
81. K. Selte, A. Kjekshus, W. E. Jamison, A. F. Andresen, and J. E. Engebretsen, *Acta Chem. Scand.* **25**, 1703 (1971).
82. H. Holseth, A. Kjekshus, and A. F. Andresen, *Acta Chem. Scand.* **24**, 3309 (1970).
83. A. F. Andresen, J. E. Engebretsen, and J. Refsnes, *Acta Chem. Scand.* **26**, 175 (1972).
84. K. Selte, A. Kjekshus, and A. F. Andresen, *Acta Chem. Scand.* **27**, 3607 (1973).
85. A. F. Andresen and B. Van Laar, *Acta Chem. Scand.* **24**, 2435 (1970).
86. K. Selte, A. Kjekshus, and A. F. Andresen, *Acta Chem. Scand.* **26**, 3101 (1972).
87. K. Selte and A. Kjekshus, *Acta Chem. Scand.* **25**, 3277 (1971).
88. P. Coffin, A. J. Jacobson, and B. E. F. Fender, *J. Phys. C.* **7**, 2781 (1974).

89. P. SCHOBINGER-PAPAMANTELLOS, P. FISCHER, A. NIGGLI, E. KALDIS, AND V. HILDEBRANDT, *J. Phys. C.* **7**, 2023 (1974).
90. P. SCHOBINGER-PAPAMANTELLOS, P. FISCHER, O. VOGT, AND E. KALDIS, *J. Phys. C* **6**, 725 (1973).
91. B. VAN LAAR AND D. J. W. IJDO, *J. Solid State Chem.* **3**, 590 (1971).
92. F. M. R. ENGELSMAN, G. A. WEIGERS, F. JELLINEK, AND B. VAN LAAR, *J. Solid State Chem.* **6**, 574 (1973).
93. B. VAN LAAR AND F. M. R. ENGELSMAN, *J. Solid State Chem.* **6**, 384 (1973).
94. B. VAN LAAR, H. M. RIETVELD, AND D. J. W. IJDO, *J. Solid State Chem.* **3**, 154 (1971).
95. C. G. WINDSOR AND R. N. SINCLAIR, *Acta Crystallogr. A* **32**, 395 (1976).
96. K. J. H. BUSCHOW, J. P. DE JONG, H. W. ZANDBERGAN, AND B. VAN LAAR, *J. Appl. Phys.* **46**, 1352 (1975).
97. K. J. H. BUSCHOW, B. VAN LAAR, AND J. B. A. A. ELEMANS, *J. Phys. F* **4**, 1517 (1974).
98. J. B. A. A. ELEMANS AND K. H. J. BUSCHOW, *Phys. Status Solidi (a)* **24**, K125 (1974).
99. K. H. J. BUSCHOW, M. BROUHA, AND J. B. A. A. ELEMANS, *Phys. Status Solidi (a)* **30**, 177 (1975).
100. J. B. A. A. ELEMANS, K. H. J. BUSCHOW, H. W. ZANDBERGEN, AND J. P. DE JONG, *Phys. Status Solidi (a)* **29**, 595 (1975).
101. C. G. TITCOMB, A. K. CHEETHAM, AND B. E. F. FENDER, *J. Phys. C* **7**, 2409 (1974).
102. F. A. KUIJPERS AND B. O. LOOPSTRA, *J. Phys. Chem. Solids* **35**, 301 (1974).
103. A. W. HEWAT, *Nature* **246**, 90 (1973).
104. D. L. DECKER, R. A. BEYERLEIN, G. ROULT, AND T. G. WORLTON, *Phys. Rev. B* **10**, 3584 (1974).
105. R. B. VON DREELE, W. S. GLAUNSINGER, A. L. BOWMAN, AND J. L. YARNELL, *J. Phys. Chem.* **79**, 2992 (1975).
106. H. J. BUSER, A. LUDI, P. FISCHER, T. STUDACH, AND B. W. DALE, *Z. Phys. Chem. (Neue Folge)* **92**, 354 (1974).
107. H. U. GÜDEL, A. LUDI, AND P. FISCHER, *J. Chem. Phys.* **56**, 674 (1972).
108. G. KEMPER, A. VOS, AND H. M. RIETVELD, *Canad. J. Chem.* **50**, 1134 (1972).
109. J. B. A. A. ELEMANS, B. VAN LAAR, AND B. O. LOOPSTRA, *Physica* **57**, 215 (1972).
110. D. ARMYTAGE AND B. E. F. FENDER, *Acta Crystallogr. B* **30**, 809 (1974).
111. H. K. KOSKI, *Acta Crystallogr. B* **31**, 933 (1975).
112. G. AVITABILE, R. NAPOLITANO, B. PIROZZI, K. D. ROUSE, M. W. THOMAS, AND B. T. M. WILLIS, *J. Polym. Sci. (Lett.)* **13**, 351 (1975).
113. J. L. WARING AND R. S. ROTH, *Acta Crystallogr.* **17**, 455 (1964).
114. W. H. ZACHARIASEN, *Acta Crystallogr.* **1**, 265 (1948).
115. W. H. ZACHARIASEN, *Acta Crystallogr.* **1**, 285 (1948).
116. R. C. L. MOONEY, *Acta Crystallogr.* **2**, 189 (1949).
117. P. C. DEBETS, *Acta Crystallogr. B* **24**, 400 (1968).
118. J. L. HOARD AND J. D. STROUPE, USAEC Report TID-5290, Paper 45 (1958).
119. K. W. BAGNALL, D. BROWN, AND J. F. EASEY, *J. Chem. Soc. A*, 288 (1968).
120. J. H. LEVY, J. C. TAYLOR, AND P. W. WILSON, *J.C.S. (Dalton)*, 219 (1976).
121. S. SEIGEL AND D. A. NORTHROP, *Inorg. Chem.* **5**, 2187 (1966).
122. R. M. DOUGLASS AND E. STARITZKY, *Anal. Chem.* **29**, 459 (1957).
123. J. N. N. VAN VUCHT, F. A. KUIJPERS, AND H. C. A. M. BRUNING, *Philips Res. Rep.* **25**, 133 (1970).
124. J. H. WERNICK AND S. GELLER *Acta Crystallogr.* **12**, 662 (1959).
125. A. D. WADSLEY, *Acta Crystallogr.* **14**, 660 (1961).
126. B. T. M. WILLIS, Ed., *Thermal Neutron Diffraction*, Clarendon Press, Oxford (1970).
127. G. E. BACON AND R. S. PEASE, *Proc. Roy. Soc. A* **230**, 359 (1955).
128. S. IIJIMA, *J. Appl. Phys.* **42**, 5891 (1971).
129. J. M. COWLEY AND S. IIJIMA, *Z. Naturforsch. A* **27** 445 (1972).
130. M. A. O'KEEFE, *Acta Crystallogr. A* **29**, 389 (1973).
131. H. P. KLUG AND L. E. ALEXANDER, "X-ray Diffraction Procedures," 2nd edn. Wiley, New York (1959).
132. A. W. HEWAT, *Nucl. Instrum. Methods*, **127**, 361 (1975).
133. M. J. COOPER AND J. P. SAYER, *J. Appl. Cryst.* **8**, 615 (1975).
134. J. WASER, *Acta Crystallogr.* **16**, 1091 (1963).
135. T. M. SABINE AND P. J. CLARKE, *J. Appl. Cryst.*, in press.
136. G. MALMROS AND J. O. THOMAS, *J. Appl. Cryst.*, **10**, 7 (1977).
137. G. MALMROS, *Acta Chem. Scand.* **24**, 384 (1970).
138. P. E. MACKIE AND R. A. YOUNG, *Acta Crystallogr. A* **31**, S198 (1975).
139. H. MEIER-LEIBNITZ AND T. SPRINGER, *Ann. Rev. Nucl. Sci.* **16**, 207 (1966).
140. E. STEICHELE AND P. ARNOLD, *Phys. Lett. A* **44**, 165 (1973).
141. M. ZIEGLER, M. ROSENFELD, W. KÄNZIG, AND P. FISCHER, *Helv. Phys. Acta* **49**, 57 (1976).
142. D. SLEDZIEWSKA-BLOCKA AND B. LEBECH, *Acta Crystallogr. A* **32**, 150 (1976).
143. K. D. ROUSE, M. W. THOMAS, AND B. T. M. WILLIS, *J. Phys. C* **9**, L231 (1976).

144. J. C. TAYLOR AND A. B. WAUGH, *J. Solid State Chem.* **18**, 241 (1976).
145. M. W. THOMAS, *Chem. Phys. Lett.* **40**, 111 (1976).
146. A. N. CHRISTENSEN, P. HANSEN, AND M. S. LEHMANN, *J. Solid State Chem.* **19**, 299 (1976).
147. S. KLEIN AND H. WEITZEL, *Acta Crystallogr. A* **32**, 587 (1976).
148. H. BINCZYCKA, A. SZYTULA, J. TODOROVIC, T. ZALENSKI, AND A. ZIEBA, *Phys. Status Solidi (a)* **35**, K69 (1976).
149. A. AHTEE, M. AHTEE, A. M. GLAZER, AND A. W. HEWAT, *Acta Crystallogr. B* **32**, 3243 (1976).
150. A. N. CHRISTENSEN, *Acta Chem. Scand. A* **30**, 219 (1976).
151. M. R. CHOWDHURY, *Acta Crystallogr. B* **32**, 2728 (1976).
152. B. O. LOOPSTRA, J. C. TAYLOR, AND A. B. WAUGH, *J. Solid State Chem.* **20**, 9 (1977).